Supplementary Material

Figure S1

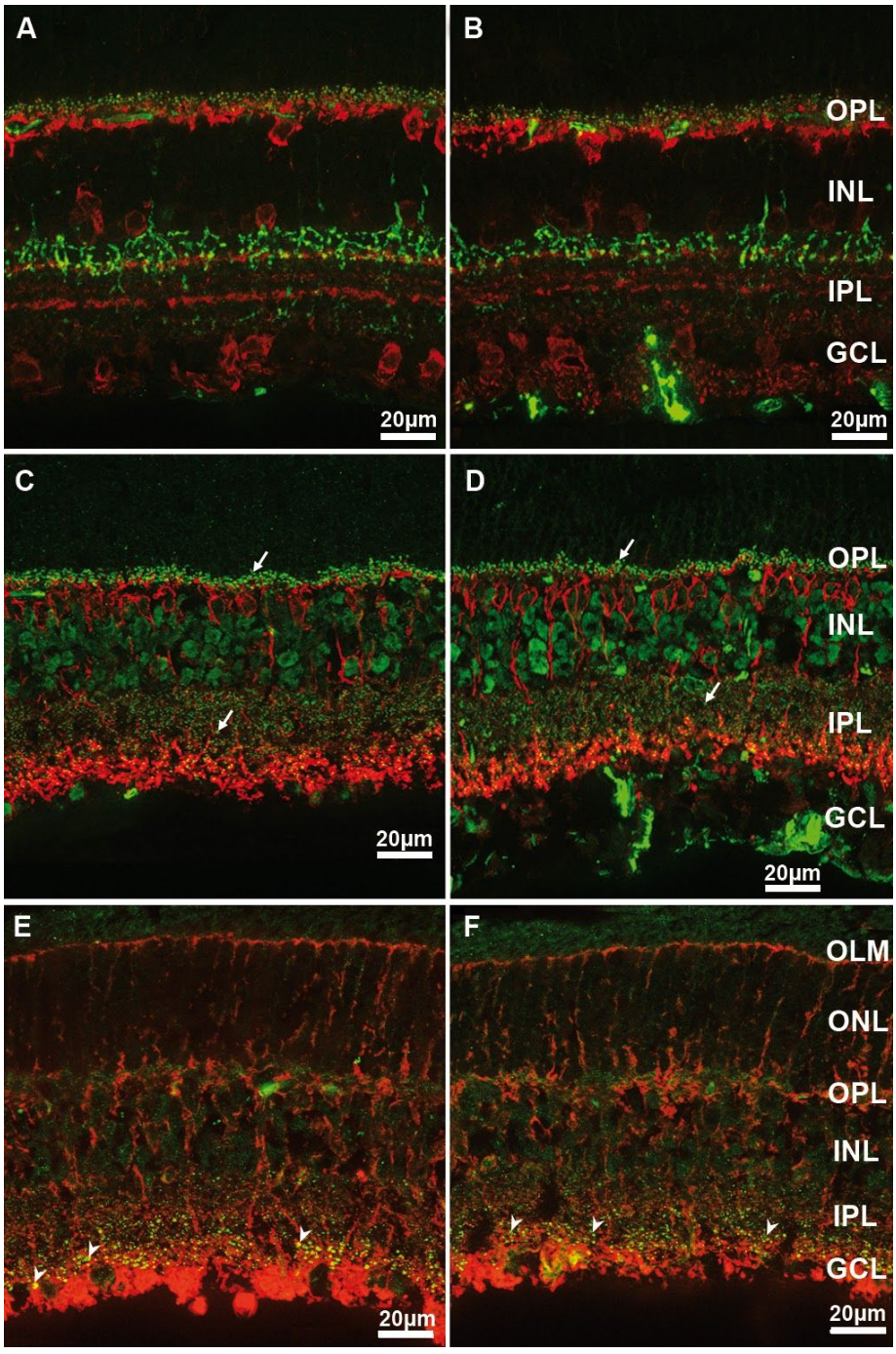

Figure S1. Immunofluorescence images of vertical sections of the retina from CDKL5$^{+/y}$ (left column) and CDKL5$^{-/y}$ (right column) mice, stained with antibodies labeling different retinal cell types and showing normal laminar organization, overall morphology, and structural features. (A,C,E: WT, CDKL5$^{+/y}$ control mice; B,D,F: mutant CDKL5$^{-/y}$ mice). **(A,B)** CalbindinD staining of horizontal cells and amacrine cells (red signal); ZNP1/Synaptotagmin staining of type 2 cone bipolar cells and axonal endings of type 6 cone bipolar cells (green signal) (OPL=outer plexiform layer; INL=inner nuclear layer; IPL=inner plexiform layer; GCL=ganglion cell layer). **(C,D)** PKCα staining of rod bipolar cells (red signal), in combination with CtBP2/RIBEYE labeling of ribbon synapses (arrows) in the outer and inner plexa of the retina (green signal). **(E,F)** GS staining of Müller glial cells (red signal), in combination with Connexin36 labeling of gap-junctions (arrowheads) in the inner plexiform layer of the retina (green signal) (OLM=outer limiting membrane).

Figure S2

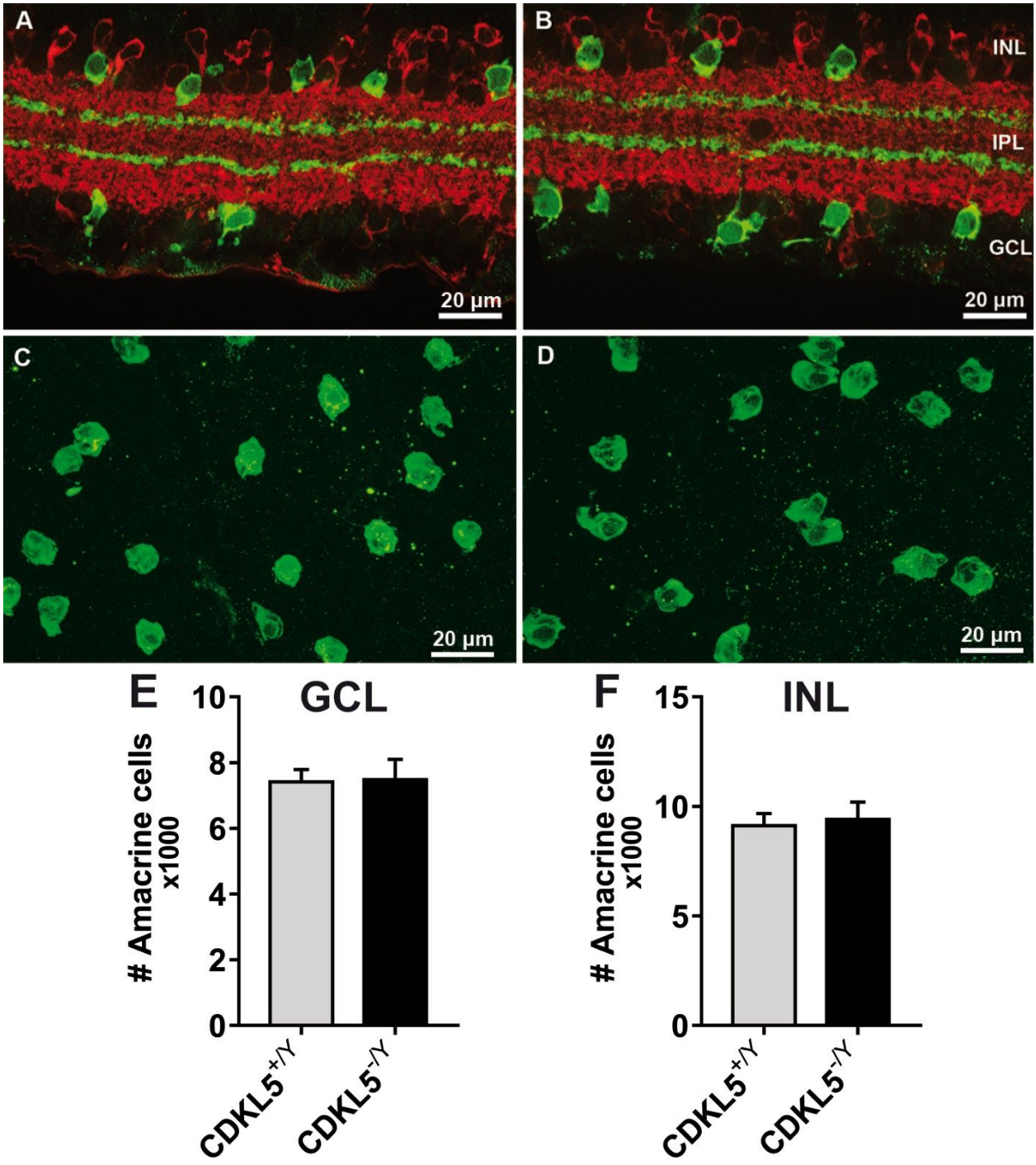

Figure S2. Quantitative data from CDKL5$^{+/y}$ (A,C) and CDKL5$^{-/y}$ (B,D) mice show no statistically significant differences in cholinergic amacrine cell numbers. **A,B:** Vertical sections of GAD67 positive GABA-ergic amacrine cells (red signal) alongside ChAT

positive cholinergic amacrine cells (green signal) display normal organization in the retina of both experimental groups. Cholinergic amacrine dendrites form two characteristic bands in the IPL, indistinguishable in the two groups. **C,D:** Representative images of retinal cholinergic amacrine cells following anti-ChAT antibody staining of retinal whole mount in CDKL5$^{+/y}$ (C) and CDKL5$^{-/y}$ (D) samples respectively. **E,F:** Quantitation of the total number of amacrine cells positioned in both GCL (E) and INL (F). No differences were found between the two groups (two-tailed unpaired t-test; P≥0,5; n=3)

Figure S3

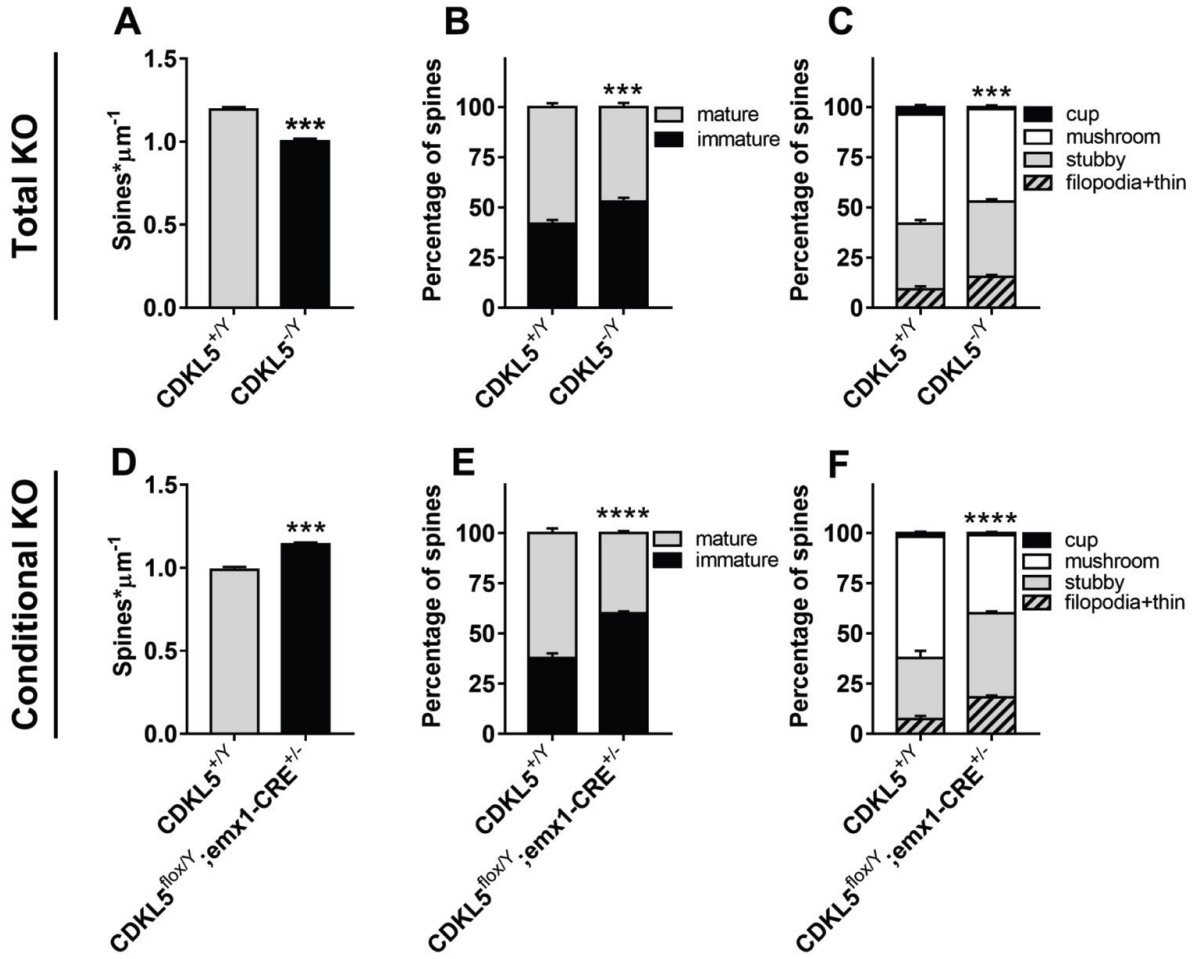

Figure S3: Morphological analysis of dendritic spines in layer 5 of the primary visual cortex. **A:** Quantitation of spine density in Golgi stained V1 slices showing a reduction in CDKL5$^{-/y}$ mice. (two-tailed Student's t-test p<0.001) **B:** Quantitation of the relative proportion of mature and immature spines in Golgi stained V1 slices showing an increased fraction of immature spines in CDKL5$^{-/y}$ mice. (χ2 test p<0.001) **C:** Quantitation of spine morphology in Golgi stained V1 slices showing a pattern of decreased morphological maturity in CDKL5$^{-/y}$ mice. (χ2 test p<0.001). **D:** Quantitation of spine density in Golgi stained V1 slices showing an increase in conditional KO, double transgenic (CDKL5$^{flox/y}$;emx1-CRE$^{+/-}$) mice. (two-tailed Student's t-test p<0.001) **E:** Quantitation of the relative proportion of mature and immature spines in Golgi stained V1 slices showing an increased fraction of immature spines in cKO (CDKL5$^{flox/y}$;emx1-CRE$^{+/-}$) mice. (χ2 test p<0.001) **F:** Quantitation of spine morphology in Golgi stained V1 slices showing a pattern of decreased morphological maturity in cKO (CDKL5$^{flox/y}$;emx1-CRE$^{+/-}$) mice. (χ2 test

p<0.001).

Figure S4

FigureS4: Schematic representation of the areas of the brain interested by CRE-dependent recombination in the emx1-CRE driver line